The Company of **Biologists**

RESEARCH ARTICLE

A discrete interface in matrix stiffness creates an oscillatory pattern of endothelial monolayer disruption

Jacob A. VanderBurgh[1,2], Archit V. Potharazu[2], Samantha C. Schwager[2] and Cynthia A. Reinhart-King[1,2,*]

ABSTRACT

Intimal stiffening upregulates endothelial cell contractility, disrupting barrier integrity; however, intimal stiffening is non-uniform. The impact of local changes in intimal stiffness on proximal and distal cell–cell interactions is unknown. To investigate the range at which matrix stiffness heterogeneities impact neighboring endothelial cells within a monolayer, we built a micropillar system with adjacent regions of stiff and compliant matrix. The stiffness interface results in an oscillatory pattern of neutrophil transendothelial migration, symmetrical about the interface and well-fit by a sinusoid function. 'Peaks' of the sinusoid were found to have increased cellular contractility and decreased barrier function relative to 'troughs' of the sinusoid. Pharmacological modulation of contractility was observed to break symmetry, altering the amplitude and wavelength of the sinusoid, indicating that contractility may regulate this effect. This work illuminates a novel biophysical phenomenon of the role of stiffness-mediated cell–matrix interactions on cell–cell interactions at a distance. Additionally, it provides insight into the range at which intimal matrix stiffness heterogeneities will impact endothelial barrier function and potentially contribute to atherogenesis.

KEY WORDS: Heterogeneity, Stiffness, Endothelial, Barrier integrity, Mechanotransduction

INTRODUCTION

Extracellular matrix stiffening accompanies a wide range of diseases, including cancer and diabetes, as well as cardiovascular diseases, including atherosclerosis and hypertension, while altered tissue mechanics often drive further pathology by altering cellular behavior (Paszek et al., 2005; Bordeleau et al., 2017; Zanotelli and Reinhart-King, 2018; Janmey et al., 2019). Intimal stiffening precedes cardiovascular pathologies, while vascular stiffening occurs with age and independently predicts risk of cardiovascular diseases (Blacher et al., 1999; Sutton-Tyrrell et al., 2005; Weisbrod et al., 2013). Endothelial cells, which regulate the semipermeable vascular barrier, respond to intimal stiffening by exhibiting increased cellular contractility, increased endothelial permeability and enhanced leukocyte transmigration, which are hallmarks of atherosclerosis (Huynh et al., 2011; Stroka and Aranda-Espinoza, 2011; VanderBurgh and Reinhart-King, 2018). However, intimal stiffening is known to be non-uniform with age, characterized by greater spatial heterogeneity in matrix stiffness (Kohn et al., 2016),

and it is unclear how the endothelium responds to heterogeneous intimal stiffness.

Recently, we reported that endothelial monolayers display an integrated response to closely spaced matrix stiffness heterogeneities (VanderBurgh et al., 2018). Endothelial monolayers cultured on micropillar substrates that permitted each cell to simultaneously contact both stiff and compliant matrix adopted the phenotype associated with the stiffest matrix encountered, exhibiting similarly elevated cell contractility and barrier disruption to homogeneously stiff controls. Furthermore, subcellular metrics of contractility, such as focal adhesion size and quantity, were identical within regions of the cell body positioned over stiff matrix relative to compliant matrix. This behavior of cells within monolayers contrasts with the behavior of single cells that are in simultaneous contact with both a stiff and a compliant matrix. In single cells, focal adhesion size and traction stresses reflect the local matrix stiffness: larger adhesions and traction stresses exist within regions of the cell body positioned over stiff matrix relative to regions of the cell body positioned over compliant matrix (Breckenridge et al., 2013; Lampi et al., 2017).

The integrated response of endothelial monolayers to heterogeneous matrix rigidity is consistent with previous studies demonstrating that the endothelium is mechanically interconnected via the actin cytoskeleton and mechanosensitive adherens junctions (Lampugnani et al., 1995; Liu et al., 2010; Giannotta et al., 2013). Moreover, previous work has found that mechanical perturbations can introduce long-range remodeling of endothelial adherens junctions (Barry et al., 2015). Magnetic twisting cytometry of VE-cadherin-coated ferromagnetic beads was found to trigger endothelial remodeling and intercellular gap formation not only at the bead-laden cell but also up to three cell lengths away. These results suggest that local mechanical perturbations can be transmitted to distal regions of the monolayer. Consistent with these results, introduction of single-cell mechanical defects into epithelial monolayers caused reduced force propagation that dissipated within 100 μm of the compromised cell (Armiger et al., 2018). Given these results, the localized elevations in matrix stiffness that are observed during aging (Kohn et al., 2016) could introduce mechanical perturbations through upregulated actomyosin contractility that could impact proximal and distal endothelial monolayer integrity. However, the range at which a matrix stiffness perturbation might impact neighboring cells within an endothelial monolayer and whether functional differences in barrier integrity would develop from such stiffness perturbations is unknown.

Here, we designed and implemented a micropillar model of a single, discrete interface in matrix stiffness to investigate the range at which matrix stiffness heterogeneity impacts distal endothelial barrier integrity. Endothelial barrier integrity was spatially characterized using neutrophil transmigration assays and complemented by characterization of cell–matrix and cell–cell interactions at vinculin-labeled adhesions. Surprisingly, we found that endothelial monolayers developed an oscillatory pattern of neutrophil transendothelial migration (TEM), symmetric about the matrix stiffness interface and

[1]Nancy E. and Peter C. Meinig School of Biomedical Engineering, Cornell University, Ithaca, NY 14853, USA. [2]Department of Biomedical Engineering, Vanderbilt University, Nashville, TN 37235, USA.

*Author for correspondence (cynthia.reinhart-king@vanderbilt.edu)

C.A.R.-K., 0000-0001-6959-3914

well-fit by a sinusoid function. Notably, the oscillatory pattern of barrier disruption was mirrored by an oscillatory pattern of focal adhesion density, vinculin recruitment to adherens junctions and vinculin lifetime at focal adhesions, showing that focal adhesions and adherens junctions are remodeling at the same regions as sites of barrier disruption. Together, these results reveal a novel form of cell–cell communication within endothelial monolayers and provide insight into the impact of age-related intimal stiffness heterogeneities upon endothelial barrier function during atherogenesis.

RESULTS
A discrete interface in matrix rigidity creates an oscillatory pattern of neutrophil TEM

To investigate the range at which a transition in matrix stiffness impacts neighboring cells, we designed a micropillar array

consisting of a large region of tall pillars adjacent to a large region of co-planar shorter pillars (Fig. 1A) (Breckenridge et al., 2013). Micropillars permit precise geometric control of substrate stiffness because pillar height dictates the stiffness of the substrate perceived by the cells without altering cross-sectional area or ligand density available for cell adhesion (Tan et al., 2003). Micropillar diameter (2 µm) and spacing (4 µm center-to-center) were selected to permit monolayer formation, while micropillar height was tuned to control substrate rigidity (Fig. 1A,B) (Rabodzey et al., 2008; Yang et al., 2011). The micropillar height of the compliant sub-region was selected to be 9.6 µm, which corresponds to a spring constant of 2.0 nN/µm or an effective modulus of ~1.3 kPa, which roughly approximates the stiffness of young, healthy intima (Ghibaudo et al., 2008; Peloquin et al., 2011). The micropillar height of the stiff sub-region was selected to be 5.1 µm, which
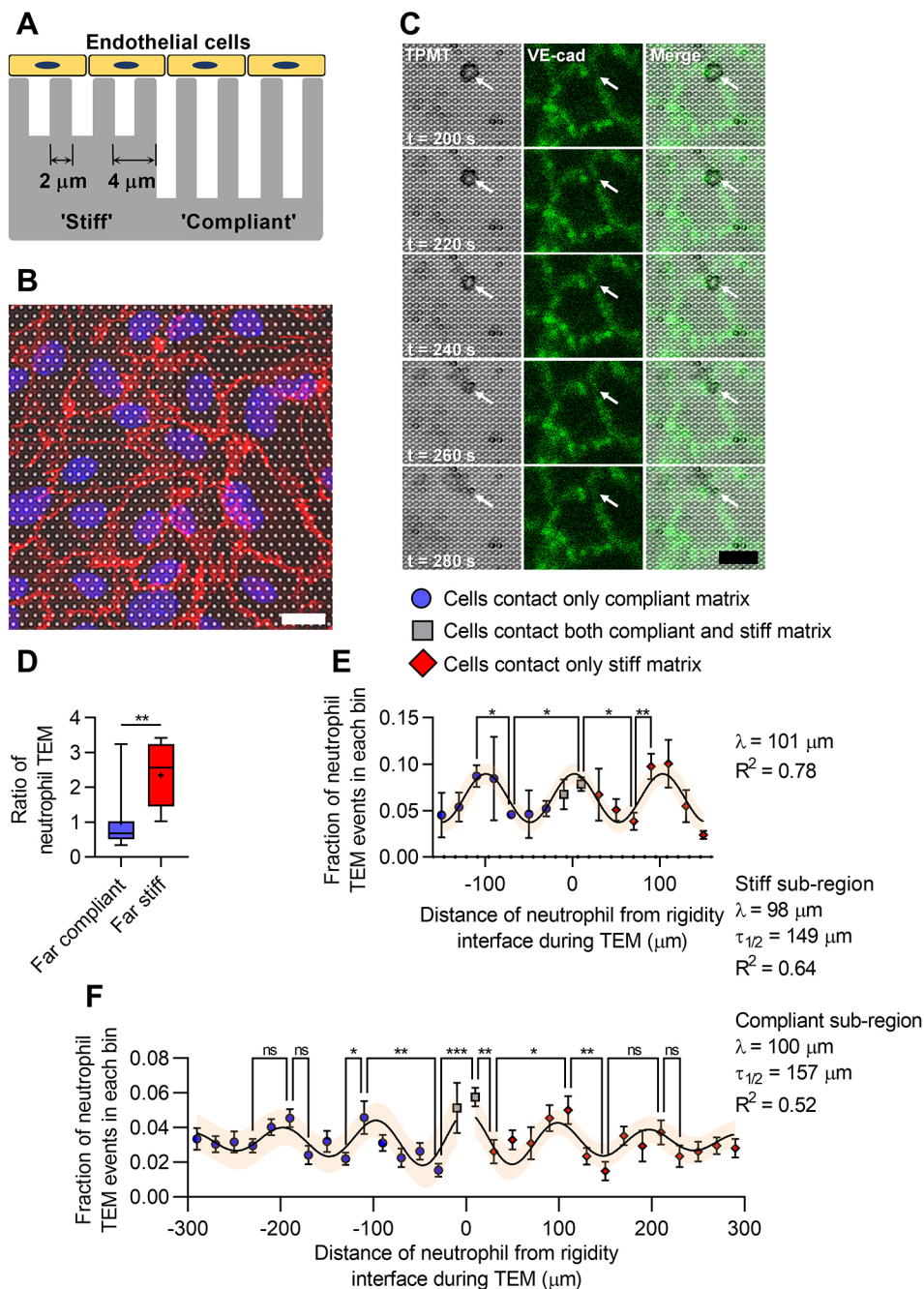

Fig. 1. Discrete interface in matrix rigidity creates oscillatory pattern of neutrophil transendothelial migration. (A) Schematic of micropillar system. (B) Representative immunofluorescence image of a human umbilical vein endothelial cell (HUVEC) monolayer on the micropillar system that represents an excess of 6-fold difference in stiffness (E_{eff}=1.3/8.6 kPa), with VE-cadherin (red), nuclei (blue) and micropillars (gray). (C) Representative time-lapse sequence of a neutrophil transendothelial migration (TEM) event. Arrows highlight neutrophil position during TEM. (D) Quantification of the ratio of neutrophil TEM events through HUVEC monolayer regions (320×320 µm sized regions for both sub-regions) on stiff and compliant matrix far (>1 mm) from the interface in matrix stiffness (n=159 neutrophil TEM events from seven substrates and eight substrates for far compliant and far stiff, respectively). (E) Quantification of the fraction of neutrophil TEM events through HUVEC monolayers, binned by distance from the interface in matrix rigidity (n=225 neutrophil TEM events from 14 substrates). (F) Quantification of fraction of neutrophil TEM events through HUVEC monolayers with an expanded field of view and binned by distance from the interface (n=787 neutrophil TEM events from 40 substrates. Data shown as median±interquartile range (box), 10th–90th percentiles (whiskers) and mean (+) (D), or mean±s.e.m. (E, F). *P<0.05; **P<0.01; ***P<0.001; ns, not significant [two-tailed Mann–Whitney test (D) or one-way ANOVA followed by Holm–Sidak's multiple comparisons test (E,F)]. Shaded region of curve-fits represents 95% confidence intervals of the curve-fit. Scale bars: 20 µm.

corresponds to a spring constant of 13 nN/μm or an effective modulus of ∼8.6 kPa and represents an excess of a 6-fold difference in stiffness. Despite the introduction of this large matrix stiffness difference, there is no change in topography because the micropillars are co-planar.

To measure the impact of the interface of substrate stiffness on endothelial barrier integrity, we first characterized TEM frequency through TNF-α-stimulated human umbilical vein endothelial cell (HUVEC) monolayers as a function of distance from the interface in matrix stiffness. Since neutrophils undergo diapedesis via the path of least resistance, choosing sites with the least junctional integrity (Martinelli et al., 2014), measuring neutrophil TEM frequency enables the spatial characterization of endothelial barrier integrity (VanderBurgh et al., 2018). Neutrophil TEM frequency has previously been found to increase as a function of substrate stiffness (Huynh et al., 2011; Stroka and Aranda-Espinoza, 2011; VanderBurgh et al., 2018). Consistent with previous reports, neutrophils induced gaps in VE-cadherin at cell–cell junctions prior to transmigration and migrated randomly underneath the endothelium after transmigration (Fig. 1C; Fig. S1, Movies 1,2) (Rabodzey et al., 2008; VanderBurgh et al., 2018). As a control, we measured the frequencies of neutrophil TEM events greater than 1 mm away from the interface with the assumption that any impact of the interface would have dissipated. This distance is in 10-fold excess of any previously reported ranges of force transmission within a monolayer in response to mechanical perturbations (Barry et al., 2015; Armiger et al., 2018). As expected, while observing TEM events 1 mm away from the interface, we observed a significantly greater ratio of neutrophil TEM events on the stiff sub-region relative to the compliant sub-region that was accompanied by slightly faster transmigration times on the stiff sub-region (Fig. 1D; Fig. S2) (Huynh et al., 2011; Stroka and Aranda-Espinoza, 2011). To evaluate the frequency of neutrophil TEM events nearby the interface, we initially focused on HUVECs within 160 μm of the interface because this corresponds to a distance of four to five cell diameters and is within the range of previous reports of endothelial force transmission (Fig. S3) (Barry et al., 2015; Armiger et al., 2018). The distance of each neutrophil TEM event with respect to the interface was recorded and binned to calculate the ratio of neutrophil TEM events that occurred as a function of distance from the interface. Surprisingly, near to the interface we observed an oscillatory pattern in the ratio of neutrophil TEM events that was well-fit by a sinusoidal function with a wavelength of 101 μm (R^2=0.78) (Fig. 1E). As a control, we verified that the oscillatory pattern was not an artifact of our binning, and that it persisted regardless of bin size (Fig. S4). As a complementary control, we asked whether an oscillatory pattern also develops parallel to the interface. We binned the y-coordinate of transmigration events in a similar manner to the x-coordinate (Fig. S5A). The y-coordinate of transmigration events showed no oscillatory pattern with a roughly flat appearance (Fig. S5B). Together, these data suggest that this oscillatory pattern in barrier disruption is not an artifact of binning or sample size.

To determine the distance at which this oscillatory pattern persists, we increased our field of view, instead measuring neutrophil TEM events up to 300 μm from the single interface. Oscillations persisted up to ∼150–200 μm from the single interface, dampening with distance with a characteristic half-life of ∼150 μm (Fig. 1F). To determine whether the magnitude of the stiffness difference at the interface impacted the oscillatory behavior, we fabricated two additional single interface substrates, keeping the rigidity of the compliant sub-region roughly constant and increasing

the rigidity of the stiff sub-region to an effective modulus of 18 kPa or 32 kPa (E_{eff}=1.2/18 kPa and E_{eff}=1.1/32 kPa). Despite increasing the stiffness difference from 6-fold to 15-fold and 30-fold, the oscillatory behavior persisted with a similar wavelength of 101 μm and 111 μm, respectively (Fig. 2). Thus, the frequency of the oscillations appears to be independent of the difference between the magnitudes of stiffness in the compliant and stiff sub-regions. Overall, these data suggest that a discrete interface in matrix rigidity causes an oscillatory pattern of barrier disruption to develop that persists beyond the range of previous reports of endothelial force transmission.

Islands of increased rigidity are sufficient to recreate the oscillatory pattern of neutrophil TEM

Given the oscillatory phenomenon observed in our single interface system, we next sought to better understand whether this phenomenon is relevant to physiological age-related heterogeneous intimal stiffening. We re-designed the micropillar platform to more closely mimic the previously reported 'hot-spots' of increased intimal stiffness, introducing 12×12 μm (subcellular-sized; E_{eff}=3.3/25 kPa),
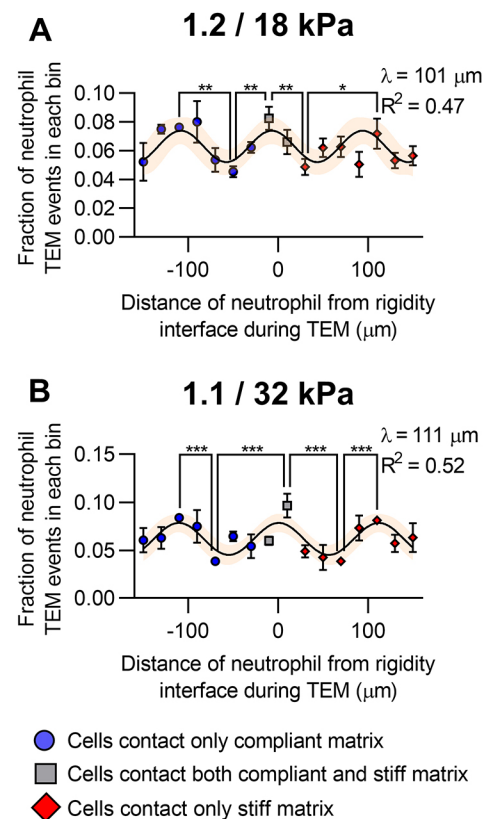

Fig. 2. The magnitude of the matrix stiffness difference does not significantly alter oscillatory behavior. (A) Quantification of fraction of neutrophil TEM events through HUVEC monolayers seeded on 1.2/18 kPa interface substrates, representing a 15-fold difference in stiffness. Neutrophil TEM events are binned by distance from the interface in matrix rigidity (n=991 neutrophil TEM events from 22 substrates). (B) Quantification of fraction of neutrophil TEM events through HUVEC monolayers seeded on 1.1/32 kPa interface substrates, representing a 30-fold difference in stiffness. Neutrophil TEM events are binned by distance from the interface in matrix rigidity (n=669 neutrophil TEM events from 19 substrates). Data shown as mean±s.e.m. *P<0.05; **P<0.01; ***P<0.001 (one-way ANOVA followed by Holm–Sidak's multiple comparisons test). Shaded region of curve-fits represents 95% confidence intervals of the curve-fit.

60×60 μm (size of 2–3 cells; E_{eff}=2.9/21 kPa), and 100×100 μm (size of 5–6 cells; E_{eff}=2.9/23 kPa) islands of increased stiffness (Fig. 3A–C) (Kohn et al., 2016). Islands of increased rigidity introduced an ~8-fold stiffness difference and were surrounded by large regions of compliant micropillars. To spatially analyze endothelial barrier integrity, we measured the ratio of neutrophil transmigration events as a function of distance from the edge of the rigidity islands. The 12×12 μm rigidity island exhibited a noisy, complex and long-ranged oscillatory pattern of neutrophil transmigration which could be the result of varying degrees of cell contact with the subcellularly sized rigidity island (Fig. 3A). In contrast, the 60×60 μm and 100×100 μm rigidity islands exhibited more regular, sinusoidal patterns of neutrophil transmigration with a wavelength of ~100 μm that strongly resembled the pattern observed

Fig. 3. Islands of increased rigidity are sufficient to recreate oscillatory pattern in neutrophil TEM. (A) Representative image of an endothelial monolayer on a 12×12 μm rigidity island substrate with quantification of fraction of neutrophil TEM events, binned by distance from interface in matrix stiffness (*n*=1196 neutrophil TEM events from 11 substrates). (B) Representative image of an endothelial monolayer on a 60×60 μm rigidity island substrate with quantification of fraction of neutrophil TEM events, binned by distance from interface in matrix stiffness (*n*=2109 neutrophil TEM events from 15 substrates). (C) Representative image of an endothelial monolayer on a 100×100 μm rigidity island substrate with quantification of fraction of neutrophil TEM events, binned by distance from interface in matrix stiffness (*n*=2042 neutrophil TEM events from 16 substrates). VE-cadherin (red), nuclei (blue) and micropillars (gray). The yellow dotted line highlights the interface separating the stiff and compliant sub-regions. Data shown as mean±s.e.m. *P<0.05 (one-way ANOVA followed by Holm–Sidak's multiple comparisons test).

with our single interface substrate (Fig. 3B,C). These results indicate that isolated islands of increased matrix stiffness are sufficient to recreate the oscillatory pattern of neutrophil TEM observed in the single interface system and suggest that oscillatory patterns of barrier disruption could be relevant to age-related heterogeneous intimal stiffening.

Vinculin remodels within focal adhesions and adherens junctions in a sinusoidal pattern in response to an interface in matrix rigidity

Given that endothelial monolayer integrity is regulated in part by actomyosin contractility, we hypothesized that our oscillatory patterns of barrier disruption would be mirrored by oscillatory patterns of cellular contractility (Huynh et al., 2011; Krishnan et al., 2011; Stroka and Aranda-Espinoza, 2011; Urbano et al., 2017). To spatially characterize contractility, we investigated the morphology of vinculin-labeled focal adhesions and adherens junctions, which are known to remodel in response to force (Riveline et al., 2001; Liu et al., 2010; Huveneers et al., 2012).

We immunostained VE-cadherin, to label intercellular boundaries, and vinculin, to label focal adhesions in HUVEC monolayers cultured on the single interface substrate (E_{eff}=1.3/8.6 kPa) (Fig. 4A). VE-cadherin staining was used as a mask to remove vinculin recruited to adherens junctions, and vinculin staining was subjected to several rounds of image processing to measure focal adhesion density (focal adhesion count per cell/cell area). Previously, we have correlated increased focal adhesion density with increased actomyosin contractility and endothelial barrier disruption (VanderBurgh et al., 2018). As a control and consistent with previous reports, far from the interface (>1 mm), focal adhesion density was significantly increased within regions of the monolayer positioned over stiff matrix relative to those over compliant matrix (Fig. 4B) (Andresen Eguiluz et al., 2017; VanderBurgh et al., 2018). Notably, near to the interface, focal adhesion density displayed an oscillatory pattern (Fig. 4C) that was well correlated with the pattern of neutrophil TEM events (λ=82 μm, R^2=0.65). We next confirmed these results by measuring focal adhesion density within another endothelial cell type, bovine aortic endothelial cells (BAECs), seeded on our single interface substrates (Fig. S6A). In comparison to HUVECs, cells within BAEC monolayers were found to be slightly smaller (~10%) and also exhibited larger focal adhesion densities (2-fold higher) (Fig. S6A,B). Far from the interface (>1 mm), we observed significantly increased focal adhesion density on stiff matrix relative to that on compliant matrix (Fig. S6C). Interestingly, nearby the interface, focal adhesion density was also observed to be oscillatory, with a wavelength of 72 μm and 77 μm on the compliant and stiff sub-regions, respectively (R^2=0.99) (Fig. S6D). Overall, the similar oscillatory patterns of focal adhesion density within HUVEC and BAEC monolayers suggests that an interface in matrix rigidity creates an oscillatory pattern of cellular contractility that correlates with oscillations in barrier disruption.

Given that our focal adhesion density measurement indicates that oscillations in TEM correlate with oscillations in cell contractility, we characterized the mechanical state of endothelial adherens junctions within HUVEC monolayers. Previous studies have established that vinculin is recruited to adherens junctions under elevated tension, while increased matrix stiffness has also been reported to increase vinculin recruitment to adherens junctions and correlate with increased endothelial permeability (Le Duc et al., 2010; Huveneers et al., 2012; Lampi et al., 2016; Urbano et al., 2017; VanderBurgh et al., 2018). We measured vinculin recruitment to adherens junctions via immunofluorescence through measurement of the
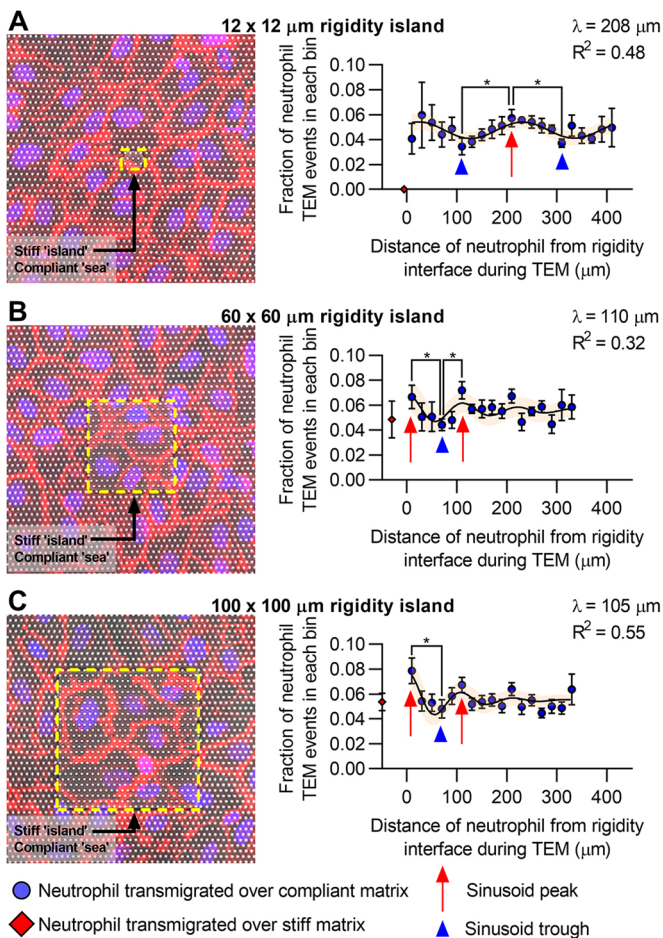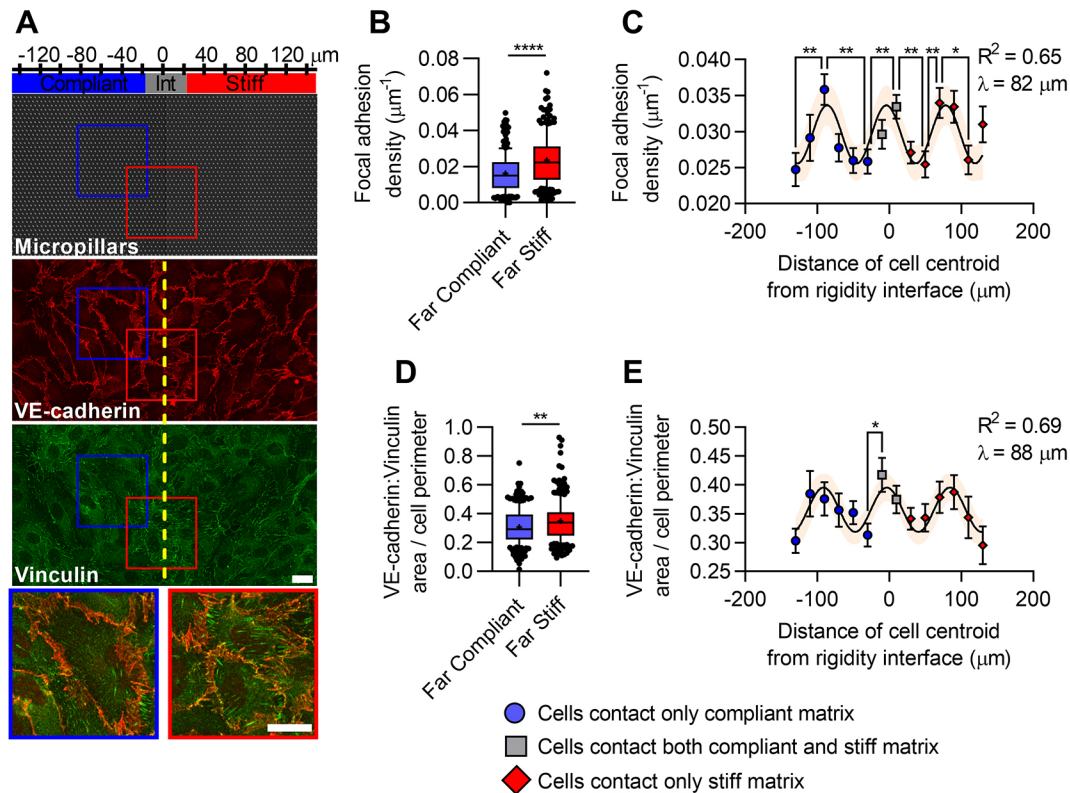
Fig. 4. Focal adhesion density and vinculin recruitment to adherens junctions display oscillatory pattern near to the interface in matrix rigidity.
(A) Representative images of HUVEC monolayers immunostained for VE-cadherin (red) and vinculin (green) with micropillars (gray). (B) Quantification of focal adhesion density within cells in the monolayer far (>1 mm) from the interface in matrix stiffness (n=252 cells from four substrates for far compliant and 230 cells from four substrates for far stiff). (C) Quantification of focal adhesion density binned by distance of cell centroid from the interface in matrix rigidity (n=465 cells from four substrates). (D) Quantification of normalized vinculin recruitment to adherens junctions far (>1 mm) from the interface in matrix stiffness (n=265 cells from four substrates for far compliant and 236 cells from four substrates for far stiff). (E) Quantification of normalized vinculin recruitment to adherens junctions, binned by distance of cell centroid from single interface in matrix rigidity (n=465 cells from four substrates). Data shown as median±interquartile range (box), 10th–90th percentiles (whiskers) and mean (+) (B,D), or mean±s.e.m. (C,E). *P<0.05; **P<0.01; ****P<0.0001 [two-tailed Mann–Whitney test (B,D), one-way ANOVA followed by Holm–Sidak's multiple comparisons test (C), or two-tailed Student's t-test (E)]. Shaded region of curve-fits represents 95% confidence intervals of the curve-fit. Scale bars: 20 µm.

colocalization area of VE-cadherin and vinculin (Fig. 4A). To reduce noise, the colocalization area between VE-cadherin and vinculin was normalized to the length of the cell's perimeter. Similar to what was found in previous studies, far from the interface (>1 mm), the normalized VE-cadherin–vinculin colocalization area was significantly greater on stiff matrix relative to that on compliant matrix (Fig. 4D) (Lampi et al., 2016; Urbano et al., 2017; VanderBurgh et al., 2018). Near to the interface, the normalized VE-cadherin–vinculin colocalization area showed an oscillatory pattern consistent with our previous datasets described above (Fig. 4E) (λ=88 µm, R^2=0.69). Consistent patterns of focal adhesion density and VE-cadherin–vinculin colocalization reinforced our hypothesis that the interface is creating oscillatory patterns of cellular contractility.

To build on our mechanical analyses, we characterized the mechanical state of vinculin within focal adhesions through analysis of vinculin mobility using fluorescence localization after photo-activation (FLAP). Previous work has identified that the half-life of vinculin at focal adhesions increases within cells on a stiffer matrix, which is reflective of the activation state of vinculin (Atherton et al., 2015; Stutchbury et al., 2017). Increased matrix stiffness is known to elevate Rho-mediated actomyosin contractility, and it is hypothesized that this contractility increases tension across the focal adhesion, increasing vinculin activation, and ultimately

stabilizing vinculin within the focal adhesion (Stutchbury et al., 2017). To measure vinculin turnover within focal adhesions, we expressed vinculin fused to a photo-activatable fluorescent probe and used FLAP to measure the half-life of vinculin within centrally located focal adhesions within cells in HUVEC monolayers (Fig. 5A,B). As a control, and consistent with previous reports, far from the interface (>1 mm), the vinculin half-life within focal adhesions was significantly increased within monolayer regions located on stiff matrix relative to that seen on compliant matrix (Fig. 5C) (Stutchbury et al., 2017). Near the interface, we observed a distinct oscillatory pattern of vinculin half-life at focal adhesions that was well-fit by a sinusoidal function and consistent with previous oscillatory data (Fig. 5D) (λ=96 µm, R^2=0.59). Oscillatory patterns in vinculin half-life suggest that oscillatory patterns of cell–matrix tension develop in response to the stiffness interface. Taken together, mechanical characterizations of focal adhesions and adherens junctions indicates that the peaks and troughs observed in barrier disruption also represent peaks and troughs in actomyosin contractility.

The discrete interface in matrix stiffness modulates the structure of endothelial monolayers
Given that we have observed oscillatory patterns in cell contractility, and noting that cell contractility often alters morphological features
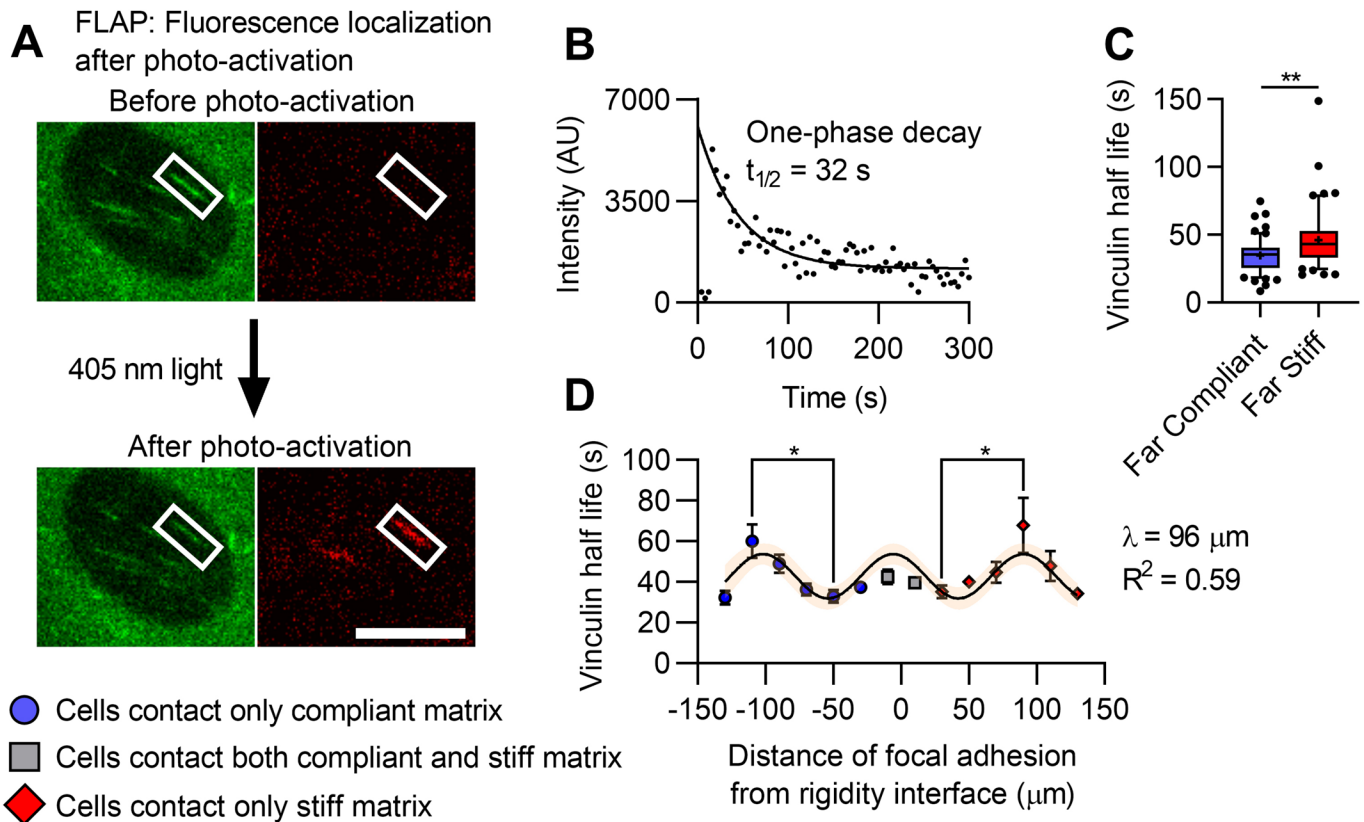
Fig. 5. Vinculin lifetime at focal adhesions displays oscillatory pattern near to the interface in matrix rigidity. (A) Depiction of FLAP experimental setup. A representative cell expressing vinculin fused to photo-activatable probe is shown before and after photoactivation. The white box highlights the photo-activated region of interest, containing a non-peripheral focal adhesion. (B) Representative intensity curve of a photo-activated focal adhesion over time, fitted to a single exponential curve to extract the decay half-life. AU, arbitrary units. (C) Quantification of vinculin half-life at focal adhesions within cells in the monolayer far (>1 mm) from the interface in matrix stiffness (n=64 focal adhesions from five substrates for far compliant and 56 focal adhesions from five substrates for far stiff). (D) Quantification of vinculin half-life binned by distance of focal adhesion centroid from interface in matrix rigidity (n=285 focal adhesions from six substrates). Data shown as median±interquartile range (box), 10th–90th percentiles (whiskers) and mean (+) (C), or mean±s.e.m. (D). *$P<0.05$; **$P<0.01$ [two-tailed Mann–Whitney test (C) or one-way ANOVA followed by Holm–Sidak's multiple comparisons test (D)]. Shaded region of curve-fits represents 95% confidence intervals of the curve-fit. Scale bar: 10 µm.

such as cell area, we asked whether the interface in matrix stiffness altered the morphology of endothelial monolayers (Yeung et al., 2005). Previous studies have reported that single cell area increases with increasing matrix stiffness, but that cell area becomes largely independent of matrix stiffness within confluent endothelial monolayers regardless of whether cells are seeded on continuous polyacrylamide gel systems or micropillar systems (Pelham and Wang, 1997; Yeung et al., 2005; Califano and Reinhart-King, 2010; VanderBurgh et al., 2018). Here, we measured cell area within HUVEC monolayers as a function of distance from the interface in matrix stiffness and found evidence of an oscillatory effect with an approximate wavelength of 50 µm (Fig. 6A,B). Since the wavelength of the oscillatory pattern was smaller than reported for our previous parameters, bin size was reduced from 20 µm to 10 µm to prevent signal aliasing. To further address how the interface may be influencing the morphology of the monolayer, we measured cell orientation with respect to the matrix stiffness interface (Fig. 6A). Notably, we found a similarly oscillatory pattern in cell orientation as a function of distance from the interface with wavelengths of 56 µm and 67 µm on the compliant and stiff sub-regions, respectively (Fig. 6C). Taken together, the oscillatory patterns in cell area and orientation suggest that the interface in matrix stiffness partially structures the monolayer over many cell lengths.

To test the interactions between cellular contractility and the structuring effect of the interface, we moderately inhibited contractility with blebbistatin, and re-measured cellular area and orientation with respect to the interface. Oscillatory patterns in cell area persisted after blebbistatin treatment with similar amplitudes and wavelengths to those on untreated monolayers (Fig. 6D). Oscillatory patterns also persisted within cell orientation with similar amplitude and wavelength on the stiff sub-region (λ=65 µm, R^2=0.43), but the compliant sub-region exhibited oscillations with a higher wavelength than untreated monolayers (λ=99 µm, R^2=0.86) (Fig. 6E). Overall, these results imply that while oscillations in cell area are largely refractory to moderate contractility inhibition, oscillations in cell orientation appear to be regulated in part by contractility status.

Modulating contractility modulates presentation of sinusoidal signal

Noting that our mechanical characterizations of cell–cell and cell–matrix adhesions have implicated actomyosin contractility in the oscillatory phenotype, we asked whether modulating contractility would modulate the appearance of the oscillatory pattern of barrier integrity. To address this, we re-examined neutrophil transmigration frequencies within HUVEC monolayers on our single interface system in which we pre-treat monolayers with either Rho activator
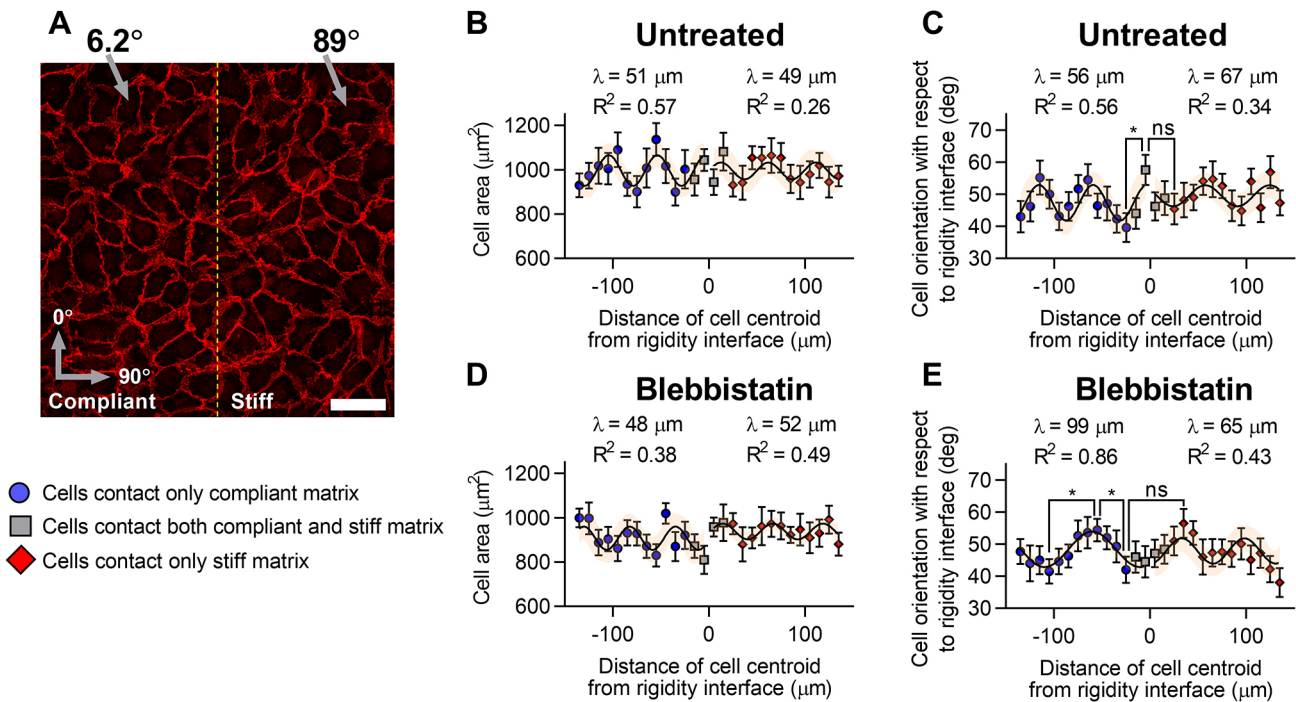
Fig. 6. The interface in matrix rigidity creates oscillatory patterns in cell area and orientation. (A) Representative image of HUVEC monolayers immunostained for VE-cadherin (red) with the rigidity interface marked by the yellow dotted line. Cell orientation was defined with respect to the interface with parallel and perpendicular cells being defined as having orientations of 0° and 90°, respectively. (B) Untreated HUVEC area and (C) orientation binned by distance of cell centroid from the interface in matrix rigidity (n=881 and 897 cells from three substrates for area and orientation measurements, respectively). (D) Blebbistatin-treated HUVEC area and (E) orientation binned by distance of cell centroid from the interface in matrix rigidity (n=953 and 958 cells from three substrates for area and orientation measurements, respectively). Data shown as median±s.e.m (B,D) or mean±s.e.m. (C,E). *P<0.05; ns, not significant (Kruskis–Wallis one-way ANOVA with Dunn's post-hoc testing). Scale bar: 50 µm.

[Rho(+)] to increase cell contractility or Y-27632 (Rho-associated protein kinase inhibitor) and blebbistatin (myosin II inhibitor) to decrease cell contractility. Treatment doses were selected to avoid significant disruption to the monolayer's integrity, which would otherwise invalidate measurement of endothelial barrier function. Consistent with previous reports, treatment with contractility modulators did not impair neutrophil transmigration (Movies 3–5) (Huynh et al., 2011; Yeh et al., 2018). However, Rho(+)-treated monolayers displayed a vastly altered pattern of neutrophil transmigration near to the interface (Fig. 7A). On the compliant sub-region, the oscillations were absent, whereas the stiff sub-region displayed a low amplitude, but persistent oscillatory pattern of neutrophil transmigration with a reduced wavelength (λ=62 µm, R^2=0.93). In contrast, monolayers treated with Y-27632 displayed a mildly asymmetric oscillatory pattern of neutrophil TEM events on both sub-regions (stiff sub-region, λ=110 µm, R^2=0.92; compliant sub-region, λ=97 µm, R^2=0.94) (Fig. 7B). However, the region in between the stiff and compliant sub-regions directly adjacent to the interface did not appear to have similar a wavelength or amplitude to the signal observed on the stiff or compliant sub-regions. Finally, monolayers treated with blebbistatin showed an asymmetric pattern of neutrophil TEM events, with high amplitude oscillations on the stiff side (λ=89 µm, R^2=0.81) while the compliant sub-region displayed minimal oscillatory behavior (Fig. 7C). Given the altered wavelengths observed after contractility modulation, we asked whether cell area or positioning would be altered in response to our treatments. Surprisingly, although our treatments altered the presentation of neutrophil transmigration curves, HUVEC area was not significantly altered (Fig. S7A). Furthermore, we found that cell positioning within the monolayer was not altered such that, on

average, four cells away from the interface was ~100 µm, regardless of the treatment condition (Fig. S7B–F). Together, these data indicate that pharmacological modulation of contractility alters the presentation of the oscillatory barrier disruption phenotype, altering the wavelength and the amplitude, but most consistently reducing the symmetry between sub-regions. Finally, the effects of contractility modulation on the oscillatory behavior appear to be independent of changes in cell area or position which are identical between treatments.

DISCUSSION
Intimal stiffening upregulates actomyosin contractility and disrupts endothelial barrier integrity; however, intimal stiffening has been shown to be spatially heterogeneous, and the range at which local elevations in matrix stiffness impact neighboring endothelial cells is largely unexplored (Huynh et al., 2011; Kohn et al., 2016). Our data indicate that an interface in matrix stiffness spatially patterns the phenotype of the surrounding endothelium generating a sinusoidal, symmetrical pattern about the interface that persists across multiple cell lengths and multiple experimental measurements (Fig. 8). 'Peaks' and 'troughs' of barrier disruption occur in the same locations as 'peaks' and 'troughs' in actomyosin contractility, while modulating actomyosin contractility altered the symmetry, amplitude and wavelength of the oscillatory pattern of barrier disruption. Together, these findings illuminate a novel biophysical phenomenon that provides insight into the range at which age-related intimal matrix stiffness heterogeneities will impact endothelial barrier function.

The symmetry, amplitude and wavelength of the oscillatory pattern were strongly altered by contractility treatments (Fig. 7).
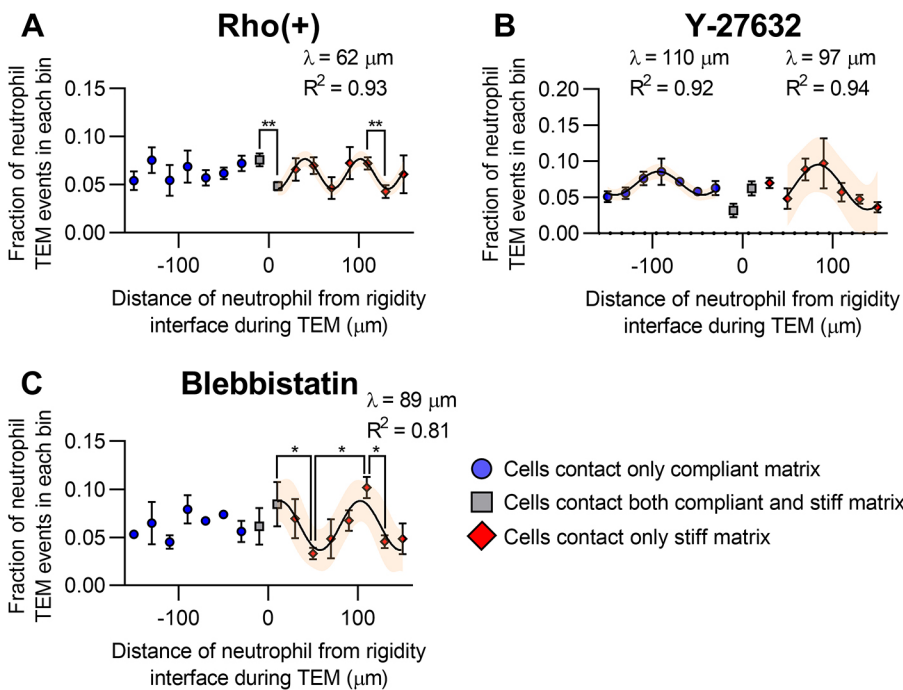
Fig. 7. Modulating contractility modulates presentation of sinusoidal signal. Quantification of fraction of neutrophil TEM events through HUVEC monolayers seeded on 1.3/8.6 kPa single interface substrates. TEM events are binned by distance from the single interface in matrix rigidity. Prior to neutrophil transmigration, monolayers were treated with (A) 3 µg/ml Rho-activator for 4 h [Rho(+); n=490 neutrophil TEM events from 36 substrates], (B) 10 µM Y-27632 for 45 min (n=691 neutrophil TEM events from 22 substrates) or (C) 50 µM blebbistatin for 1 h (n=508 neutrophil TEM events from 14 substrates). Data shown as mean±s.e.m. *P<0.05, **P<0.01 (one-way ANOVA followed by Holm–Sidak's multiple comparisons test). Shaded region of curve-fits represents 95% confidence intervals of the curve-fit.

Surprisingly, inhibition of contractility with Y-27632 and blebbistatin was insufficient to completely abrogate the oscillatory pattern of neutrophil transmigration frequency. This is a seemingly contradictory finding. However, our treatment doses were designed to be intermediate to avoid complete disruption of endothelial barrier integrity (Yao et al., 2010; Breslin et al., 2015; Rosenfeld et al., 2016). As such, we anticipate that if it were possible to completely disrupt cellular contractility without extensive monolayer disruption, the oscillatory phenotype would be ablated. Consistent with this hypothesis, blebbistatin did ablate the oscillatory phenotype on the compliant sub-region while Y-27632 greatly reduced the amplitude of the oscillatory peak on the compliant sub-region. Overall, our results indicate that cellular contractility plays a critical role in patterning the oscillatory phenotype, particularly for cells on the compliant sub-region.

Barrier disruption 'peaks' originate within cells in contact with the interface in matrix rigidity and radiate outwards symmetrically, peaking every 100 µm and dampening with distance from the interface. Translating this phenomenon to cell lengths, peaks in neutrophil transmigration are initially observed at cells in contact with the interface (0–20 µm) and again at roughly three cell diameters away (90–110 µm), while 'troughs' in neutrophil transmigration are observed at cells one to two cell diameters away (30–70 µm) (Fig. 1E; Fig. S3B). Notably, the fundamental wavelength of the signal, of ~100 µm or roughly four cell lengths, persists regardless of the matrix stiffness difference and is even reproduced in the presence of multicellular-sized islands of increased matrix rigidity (Figs 2 and 3). Interestingly, mechanical waves have been reported previously; Rodríguez-Franco et al. reported the development of long-lived oscillatory patterns of traction forces within epithelial monolayers that encountered repulsive boundaries (Rodríguez-Franco et al., 2017). Their oscillatory phenotype had a similar characteristic wavelength, of four cell lengths (52 µm for their cell type), and developed within cells seeded on a continuous surface (polyacrylamide gel), which suggests that our oscillatory phenotype is not simply an artifact of the micropillar system. However, unlike the mechanical

oscillations reported by Rodríguez-Franco et al., which did not dampen with distance from the boundary, we report that our oscillations dampen with distance with a characteristic decay half-life of ~150 µm (Fig. 1F). The difference in dampening behavior between our systems may be the result of differences in cell types examined (epithelial versus endothelial monolayers). Regardless, our reported dampening behavior is consistent with previous reports that indicate a single mechanical defect in force propagation within an epithelial monolayer decays within a distance of 100 µm (Armiger et al., 2018).

Given that our oscillatory wavelength and the wavelength of the mechanical oscillations reported by Rodríguez-Franco et al. are both approximately four cell lengths, there is clear evidence that their presentation could be influenced by cell size (Rodríguez-Franco et al., 2017). Our data from HUVEC and BAEC monolayers supports this hypothesis because cells within BAEC monolayers are ~10% smaller than cells within HUVEC monolayers and the wavelength of our focal adhesion density parameter was ~10% smaller in BAEC monolayers compared to HUVEC monolayers. In contrast, we found that the interface modulated the structure of the monolayer creating oscillatory patterns in both cell area and orientation with wavelengths that did not correspond to our reported wavelength for barrier function and contractility. As such, the relationship between cell size and the characteristic wavelength of oscillatory patterns in barrier integrity and cell contractility may be more complex than a simple correlation. In support of this hypothesis, our treatments that target contractility did not significantly alter cell area or positioning, but they did alter the wavelength of neutrophil transmigration frequencies. Cell area/positioning within monolayers may not change in response to contractility treatments because of the high degree of confluence and the moderate treatment doses. Previously, we and others have reported that cell area becomes independent of substrate stiffness once cells become confluent, suggesting that cell area within monolayers may become independent of contractility status (Yeung et al., 2005; VanderBurgh et al., 2018). Overall, the relationship between cell size and the characteristic wavelength of the oscillatory
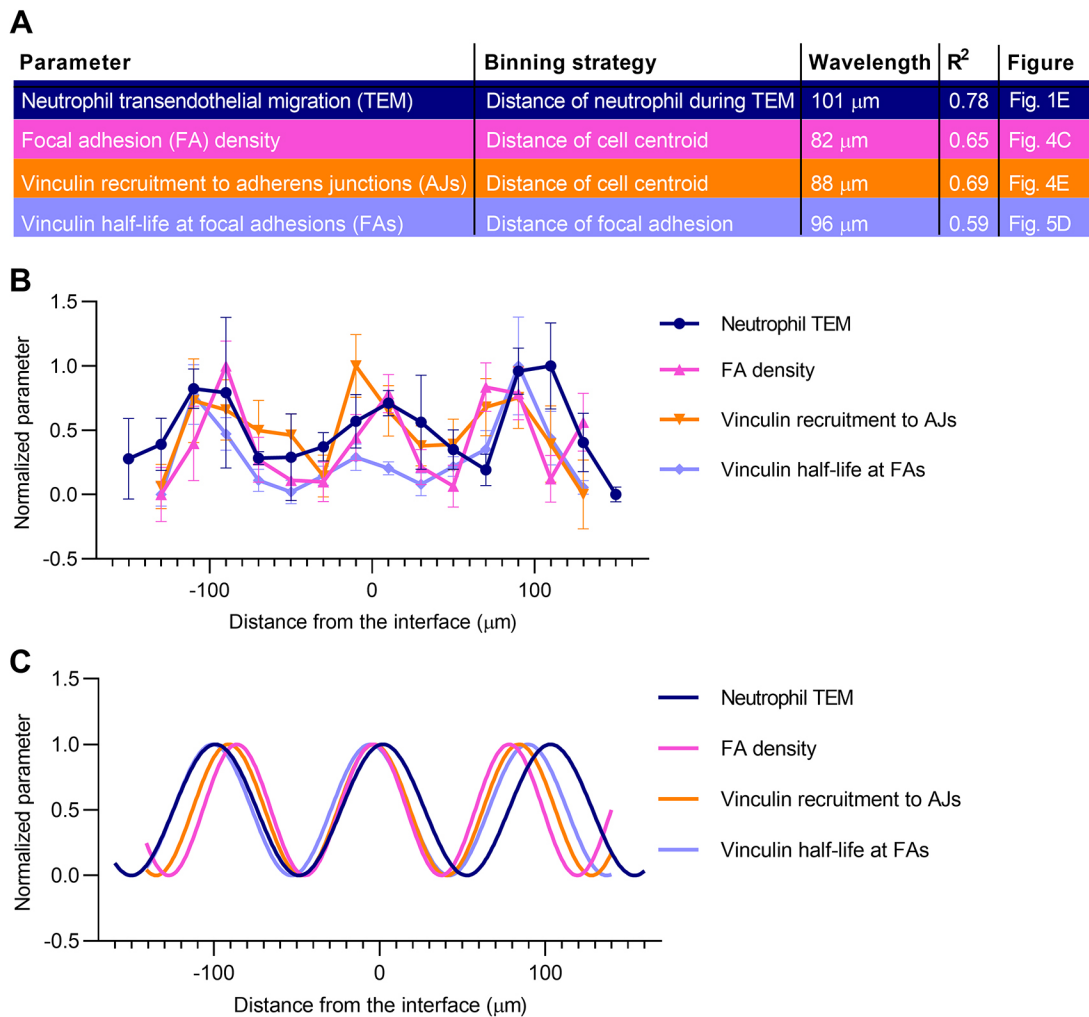
A

Parameter	Binning strategy	Wavelength	R^2	Figure
Neutrophil transendothelial migration (TEM)	Distance of neutrophil during TEM	101 μm	0.78	Fig. 1E
Focal adhesion (FA) density	Distance of cell centroid	82 μm	0.65	Fig. 4C
Vinculin recruitment to adherens junctions (AJs)	Distance of cell centroid	88 μm	0.69	Fig. 4E
Vinculin half-life at focal adhesions (FAs)	Distance of focal adhesion	96 μm	0.59	Fig. 5D

B

C

Fig. 8. Comparison of barrier integrity and cell contractility markers. (A) Table describing each metric of barrier integrity and cell contractility, the method by which each metric was binned to calculate average values, the wavelengths of sinusoidal curve-fits, coefficients of determination for sinusoidal curve-fits and figure labels describing where data is originally presented. (B) Overlaid normalized data of neutrophil TEM, focal adhesion (FA) density, vinculin recruitment to adherens junctions (AJs), and vinculin half-life at FAs. (C) Overlaid normalized sinusoidal curve-fits of neutrophil TEM, FA density, vinculin recruitment to AJs, and vinculin half-life at FAs. Data and curve-fits were normalized such that maximum and minimum values are one and zero, respectively. Data shown as mean±s.e.m. in B.

phenotype is a topic worthy of future work as a potential insight into how oscillatory patterns are established.

Among the candidate parameters that might mediate development of oscillatory patterns in cell contractility and barrier integrity, force transmission pathways at focal adhesions and adherens junctions are prime candidates. It is possible that oscillations are generated within cells contacting the interface through stiffness-sensing at focal adhesions and transmitted distally via force transmission at adherens junctions. Given that the discrete nature of micropillars precludes transmission of matrix strain and that the co-planar nature of the micropillar system precludes topographical cues, cell–cell junctions are likely candidates for transmitting signals from the interface to distal regions of the endothelium. More specifically, adherens junctions are known sites of mechanotransduction with the ability to both respond to junctional tension and transmit forces to neighboring cells (Huveneers et al., 2012; Barry et al., 2014, 2015; Angulo-Urarte et al., 2020). Future research should evaluate the contribution of individual force pathways at focal adhesions and adherens junctions. In particular, interrupting well-studied

mechanotransducers such as talin at focal adhesions or α-catenin at adherens junctions could begin to dissect the role of force transmission pathways in mediating oscillatory patterns. However, it would not be appropriate to assume that interrupting force pathways at one adhesion type would not affect the other, as there is crosstalk (Muhamed et al., 2016; Mui et al., 2016; Pulous et al., 2019). Given these adhesive structures both link to the actin cytoskeleton and recruit similar proteins, such as Rho family GTPases (Rho, Rac, and Cdc42), vinculin and focal adhesion kinase, it may not be possible to disentangle the relative contributions of individual force pathways to the oscillatory phenotype.

This mesoscale oscillatory phenomenon may be the result of force balancing between cell pairs induced by the matrix stiffness interface. Recent work has begun to explore whether force heterogeneity, as opposed to force magnitude, mediates barrier disruption. Traction force fluctuations, rather than traction force magnitudes, predict regions at which inter-endothelial gaps form upon stimulation with thrombin (Valent et al., 2016). Similarly, endothelial monolayers form large multicellular domains with aligned intercellular stresses and inter-endothelial gaps

preferentially form at the borders of these domains upon stimulation with thrombin (Hardin et al., 2018). These studies suggest that endothelial barrier integrity is not simply a product of local stresses but rather the result of long-ranged stress reorganization across the monolayer. This model is not inconsistent with the observed impacts of matrix stiffness on endothelial integrity nor our sinusoidal barrier integrity pattern observed with the interface in matrix stiffness. Increased substrate stiffness has been reported to increase the heterogeneity of intercellular stress within the endothelium, which was found to predispose the endothelium to inter-endothelial gap formation (Andresen Eguiluz et al., 2017). It is possible that heterogeneous matrix rigidity would further increase force heterogeneity within the endothelium because endothelial cells encountering a matrix stiffness disparity would be challenged to balance cues from both stiff and compliant sub-regions. Thus, the mesoscale sinusoidal pattern of barrier integrity that we observe in response to a discrete interface in matrix stiffness would be the result of increased force heterogeneity within cells in contact with the matrix stiffness interface, and at subsequent 'peaks' of the sinusoidal signal. Consistent with this hypothesis, mechanical perturbation of the endothelium with pharmacological activators or inhibitors of contractility, known to alter the balance of force within the monolayer, break the symmetry of the sinusoidal signal.

Unfortunately, in our system we are unable to directly measure traction forces or intercellular stresses because micropillar deflections are on the same order as the noise of detection in our system (Lemmon et al., 2005). Thus, we are forced to rely upon indirect, time-averaged mechanical characterizations of cell–matrix and cell–cell forces and barrier integrity measurements. However, our implementation of the micropillar system bypasses the surface topography changes between stiff and compliant sub-regions that can be found in continuous polymer systems, enabling us to test the impact of matrix stiffness disparities ranging from 6-fold to 25-fold (Breckenridge et al., 2013; Lampi et al., 2017). As a comparison, age-related intimal stiffness heterogeneities have been reported to be as high as 50-fold with stiffness values ranging from 2–100 kPa (Kohn et al., 2016). Interestingly, we found that within the stiffness differences tested (6–25-fold), the oscillatory pattern and characteristic wavelength is largely independent of the matrix stiffness disparity. The lower threshold of the stiffness difference required for oscillatory patterns is an interesting topic for future work. Identifying the sensitivity of endothelial monolayers to transitions in matrix stiffness would put into context the potential impact of smaller scale subendothelial matrix stiffness heterogeneities. *Ex vivo* characterization of subendothelial matrix has identified multiple subcellular-sized 'hotspots' of increased matrix stiffness, which could cause cooperative or emergent behaviors such as constructive or destructive interference in the sinusoidal pattern (Kohn et al., 2016). Identifying cooperative behavior using multiple stiff islands would enrich our understanding of how the oscillatory patterns observed in our micropillar system might impact endothelial barrier function *in vivo*.

In summary, these results suggest that local elevations in matrix stiffness have complex and long-ranged impacts on the barrier function of neighboring regions of the endothelium.

MATERIALS AND METHODS
Fabrication of PDMS micropillar arrays
Silicon (Si) masters of micropillar arrays were fabricated in a two-step etching process (Breckenridge et al., 2013; VanderBurgh et al., 2018). Briefly, a thin layer of photoresist (SPR220-3.0, Shipley Company, LLC, Marlborough, MA) was spun and patterned with an i-line 5X reduction

step-and-repeat projection stepper (AutoStep 200, Integrated Solutions INC, Tweksbury, MA). Cylindrical holes of uniform depth were subsequently etched using deep reactive ion etching (DRIE) utilizing the Bosch fluorine process (Unaxis 770 Deep Si Etcher, Plasma-Therm, LLC, St Petersburg, FL). DRIE etching time was carefully monitored to control hole depth. Following etching, photoresist was stripped with an oxygen ashing process in an Anatech Plasma Asher (60 min, 900 W; Anatech USA, Hayward, CA, USA). Si wafers were subsequently spin-coated with a relatively thick layer of photoresist (S1813, Shipley Company, LLC). Thick photoresist was exposed using a contact aligner (ABM-USA, San Jose, CA, USA) to pattern either islands or large regions of increased rigidity. Photoresist exposure was controlled such that photoresist on the surface of the Si wafer dissolved during development, but photoresist remained within the cylindrical holes to protect them during subsequent etching. Thus, the top surface of the Si wafer was etched in the subsequent DRIE etching step, but hole depth was not impacted. Following etching, photoresist was stripped with an identical oxygen ashing process, and Si wafers were silanized with (1H,1H,2H,2H-perfluorooctyl)trichlorosilane as an anti-stiction coating to permit polydimethylsiloxane (PDMS) release during replica-molding (MVD100, Applied Microstructures, San Jose, CA, USA). Replica-molding of Si masters was performed by pouring de-gassed prepolymer PDMS (Sylgard 184, Dow Corning, Midland, MI), curing for 12 h at 60°C, and peeling in the presence of 100% ethanol. Critical point drying (EMS 850, Electron Microscopy Sciences, Hartfield, PA) was subsequently performed to remove ethanol. Prior to seeding PDMS micropillars with cells, substrates were first treated with UV for 15 min, plasma-treated (2 min; PDC-001 Plasma Cleaner, Harrick Plasma, Ithaca, NY), uniformly coated with 200 μg ml^{-1} human fibronectin for 1 h (BD Biosciences, San Jose, CA, USA), and rinsed with PBS. Micropillar spring constants were calculated with the Euler–Bernoulli beam theory equation, which was used to estimate an effective Young's modulus (Ghibaudo et al., 2008).

Cell culture and reagents
Human umbilical vein endothelial cells (HUVECs; Lonza, Basel, Switzerland) were used from passages 4–5. HUVECs were maintained in Medium 199 (Invitrogen, Carlsbad, CA) supplemented with 1% penicillin–streptomycin (Invitrogen) and EGM BulletKits [2% (v/v) FBS, bovine brain extract, ascorbic acid, hydrocortisone, epidermal growth factor, gentamicin/amphotericin-B; Lonza]. Bovine aortic endothelial cells (BAECs; VEC technologies, Rensselaer, NY) were used from passages 7–12. BAECs were maintained in Medium 199 (Invitrogen) with 10% Fetal Clone III (HyClone, Logan, UT), 1% MEM vitamins (Medtech, Manassas, VA, USA), 1% MEM amino acids (Invitrogen) and 1% penicillin-streptomycin (Invitrogen). HEK293T cells (ATCC, Manassas, VA) were cultured in DMEM (Invitrogen) supplemented with 10% fetal bovine serum (Atlanta Biologicals, Flowery Branch, GA) and 1% penicillin-streptomycin (Invitrogen). All cells were maintained at 37°C and 5% CO$_2$. Cells were tested and found negative for mycoplasma contamination.

DNA constructs and lentiviral transductions
mEos2-Vinculin-N-21 was Addgene plasmid #57439 (deposited by Michael Davidson) and pFUW was Addgene plasmid #14882 (deposited by from David Baltimore). mEos2-Vinculin-N-21 was inserted into the empty second generation lentiviral vector, pFUW, using Gibson assembly generating pFUW-mEos2-Vinculin-N-21. Lentiviral particles were prepared through transient transfection of HEK293T cells with pFUW-mEos-2-Vinculin-N-21, psPAX2 and pMD2.G in the presence of TransIT-LT1 (Mirus Bio, LLC, Madison, WI). Lentiviral particles were harvested from spent HEK293T medium at 48 h and 72 h post transfection, concentrated 100-fold with Lenti-X Concentrator (Clontech, Mountain View, CA) and stored at 80°C. HUVECs were stably transduced in the presence of 8 μg ml^{-1} polybrene overnight (Santa Cruz Biotechnology, Dallas, TX).

Immunofluorescence
Endothelial cells were fixed with 3.7% formaldehyde (Sigma-Aldrich, St Louis, MO) and permeabilized with 1% Triton (VWR, Radnor, PA). Vinculin was immunostained with a mouse monoclonal primary antibody

(1:100, V9131, Sigma-Aldrich) and an Alexa Fluor 488-conjugated donkey anti-mouse-IgG secondary antibody (1:200, A21202, Invitrogen). VE-cadherin within HUVECs was stained with a rabbit polyclonal primary antibody (1:100, ab-33168, Abcam, Cambridge, MA) and with an Alexa Fluor 568 donkey anti-rabbit-IgG secondary antibody (1:200, A10042, Invitrogen). VE-cadherin within BAEsC was stained with a rabbit polyclonal primary antibody (1:100, #MATB886, EMD Millipore, Burlington, MA, USA) and with a donkey anti-rabbit-IgG secondary antibody (1:200, A10042, Invitrogen). Nuclei were stained with 4′,6-diamidino-2-phenylindole (1:100, DAPI; Sigma-Aldrich). Antibodies received from manufacturers were validated through observation of appropriate staining of their target antigens in immunofluorescence.

Quantification of vinculin focal adhesion density and cell–cell junction localization

Confluent monolayers of endothelial cells were fixed and immunostained with VE-cadherin to mark adherens junctions, whereas vinculin was immunostained to mark focal adhesions and vinculin recruitment to adherens junctions. Confocal Z-stack images were acquired using a Zeiss LSM 800 inverted microscope equipped with a 40×/1.1 N.A. water-immersion objective. Z-stack images were maximum intensity projected and subjected to image analysis with a custom-written MATLAB algorithm as described previously (Lampi et al., 2016; VanderBurgh et al., 2018) (v. 2013a, Mathworks, Natick, MA; algorithm available upon request). Briefly, background noise was reduced via an adaptive Wiener filter (1.6 μm filtering window for VE-cadherin and 0.8 μm filtering window for vinculin), uneven illumination was corrected via top-hat filtering (1.4 μm diameter disk), images were converted into a binary format with Otsu's method and speckle noise was reduced via median filtering (0.6 μm filtering window for VE-cadherin and 0.8 μm filtering window for vinculin). Speckle noise associated with filtering was reduced further though excluding vinculin structures smaller than 0.6 μm^2. To quantify focal adhesion density, VE-cadherin-stained adherens junctions were used as a mask to remove vinculin associated with adherens junctions. Connected component analysis was used to measure focal adhesion count per cell, and focal adhesion density was calculated by dividing focal adhesion count by cell area. To quantify VE-cadherin and vinculin colocalization, corresponding filtered images were overlaid and overlap area was measured.

Measurement of vinculin half-life at focal adhesions with FLAP

Endothelial cells stably expressing pFUW-mEos2-Vinculin-N-21 were prepared as described in the 'DNA constructs and lentiviral transductions' section. Endothelial monolayers were imaged using a Zeiss LSM 800 inverted microscope equipped with a 40×/1.1 NA water-immersion objective inside an environmentally controlled chamber. One to three mature focal adhesions, centrally located within the cell, were selected and photoactivated with 25 iterations of a 405 nm laser at 10% power with 2.94 μs pixel dwell time. Five images were acquired prior to photoactivation, and images were taken every 4 s for 5 min post photoactivation. Time-lapse movies were corrected for drifting using a custom MATLAB script (v. 2018b, Mathworks; available upon request). Photo-activation causes focal adhesions to swap from excitation at 488 nm to excitation at 568 nm. Intensity curves in the 568 nm channel were background-subtracted and normalized by their peak intensity. Normalized intensity curves were subsequently imported into MATLAB and fitted with single exponential curve fits as performed previously (Stutchbury et al., 2017). Coefficients of the curve fits were used to extract the half-time ($t_{1/2}$) of vinculin at focal adhesions.

Measurement of cell orientation and area

Confluent endothelial monolayers were fixed and immunostained with VE-cadherin to mark intercellular boundaries. Fixed monolayers were imaged using a Zeiss LSM 800 inverted microscope equipped with a 40×/1.1 NA water-immersion objective. Images were then processed with a custom MATLAB script (v. 2018b, Mathworks; available upon request) for the following analysis protocol. Cells within the monolayer were traced and cell outlines were fit to an ellipse to calculate a major and minor axis for each cell. To calculate the orientation of the cell with respect to the interface, the angle between the major axis and the interface in matrix stiffness was calculated and recorded as a function of the distance of the cell centroid from the interface. Cells with major axes parallel to the interface were defined as having an angle of 0°, while perpendicular cells were defined as having an angle of 90°. Cell outlines were also used to calculate cell area as a function of the distance of the cell centroid from the interface.

Neutrophil transmigration

All human subject protocols have been approved by the Institutional Review Board for Human Participants at Vanderbilt University and informed consent was obtained from human subjects. Primary human neutrophils were isolated as previously described (Huynh et al., 2011; VanderBurgh et al., 2018). Briefly, fresh peripheral human blood was collected into vacutainer tubes containing heparin and permitted to equilibrate at room temperature. Blood was layered over 1-Step Polymorphs (Accurate Chemical, Westbury, NY) and separated by centrifugation. The neutrophil layer was collected, contaminating red blood cells were lysed, and neutrophils were re-suspended in HBSS- (VWR). HUVEC monolayers were pretreated with recombinant human TNF-α (0.1 ng/ml; R&D Systems, Minneapolis, MN) for 6 h, prior to the addition of neutrophils (140,000 neutrophils/cm^2). To quantify the timing and location of transmigration events, neutrophils were permitted to transmigrate in an environmentally controlled chamber for 45 min while being monitored by taking time-lapse images every 20 s with a Zeiss LSM 800 inverted microscope equipped with a 10×/0.3 NA objective. To verify that transmigration events were occurring at intercellular junctions, adherens junctions of HUVECs were sometimes labeled with a non-function blocking, monoclonal antibody conjugated to Dylight-488 against domain 4 of human VE-cadherin (clone hec1) as performed previously (Ali et al., 1997; Gonzalez et al. 2016; VanderBurgh et al., 2018). Hec1–Dylight-488 was a kind gift from Dr William A. Muller (Northwestern University, Feinberg School of Medicine, Chicago, IL). To pharmacologically modulate contractility, prior to adding neutrophils, endothelial monolayers were pre-treated with Rho Activator II for 4 h (3 μg/ml; Cytoskeleton, Denver, CO), Y-27632 for 45 min (10 μM; VWR) or blebbistatin for 1 h (50 μM; Calbiochem, Darmstadt, Germany). Contractility treatments were washed out with PBS prior to addition of neutrophils. Brightfield images were used to identify the location of neutrophil transmigration events relative to matrix stiffness interfaces.

Statistical analysis

All data represent three or more independent experiments. Sample sizes and statistical comparisons are provided in the figure legends. All analyses were completed with GraphPad Prism 8 (GraphPad Software Inc, La Jolla, CA, USA). Non-linear regression was performed in GraphPad Prism using the average values of data as inputs. Data are presented as either box-and-whisker plots showing the median, 25th–75th interquartile range as the box edges, 10th–90th percentiles as the whiskers, and mean as '+', or scatter plots showing mean±s.e.m. Normality testing was performed with the D'Agonisto–Pearson omnibus test. Data were compared by either a two-tailed Student's t-test, two-tailed Mann–Whitney test, or one-way analysis of variance (ANOVA) followed by Holm–Sidak's multiple comparisons test. $P<0.05$ was considered significant. No statistical method was used to predetermine sample size.

Competing interests

The authors declare no competing or financial interests.

References

Ali, J., Liao, F., Martens, E. and Muller, W. A. (1997) Vascular endothelial cadherin (VE-cadherin): cloning and role in endothelial cell-cell adhesion. *Microcirculation* 4, 267-277. doi:10.3109/10739689709146790

Andresen Eguiluz, R. C., Kaylan, K. B., Underhill, G. H. and Leckband, D. E. (2017). Substrate stiffness and VE-cadherin mechano-transduction coordinate to regulate endothelial monolayer integrity. *Biomaterials. Elsevier Ltd* 140, 45-47. doi:10.1016/j.biomaterials.2017.06.010

Angulo-Urarte, A., Van Der Wal, T. and Huveneers, S. (2020). Cell-cell junctions as sensors and transducers of mechanical forces. *Biochim. Biophys. Acta* 1862, 183316. doi:10.1016/j.bbamem.2020.183316

Armiger, T. J., Lampi, M. C., Reinhart-King, C. A. and Dahl, K. N. (2018). Determining mechanical features of modulated epithelial monolayers using subnuclear particle tracking. *J. Cell Sci.* 131, jcs216010. doi:10.1242/jcs.216010

Atherton, P., Stutchbury, B., Wang, D.-Y., Jethwa, D., Tsang, R., Meiler-Rodriguez, E., Wang, P., Bate, N., Zent, R., Barsukov, I. L. et al. (2015). Vinculin controls talin engagement with the actomyosin machinery. *Nat. Commun.* 6, 1-12. doi:10.1038/ncomms10038

Barry, A. K., Tabdili, H., Muhamed, I., Wu, J., Shashikanth, N., Gomez, G. A., Yap, A. S., Gottardi, C. J., De Rooij, J., Wang, N. et al. (2014). α-Catenin cytomechanics: role in cadherin-dependent adhesion and mechanotransduction. *J. Cell Sci.* 127, 1779-1791. doi:10.1242/jcs.139014

Barry, A. K., Wang, N. and Leckband, D. E. (2015). Local VE-cadherin mechanotransduction triggers long-ranged remodeling of endothelial monolayers. *J. Cell Sci.* 128, 1341-1351. doi:10.1242/jcs.159954

Blacher, J., Asmar, R., Djane, S., London, G. M. and Safar, M. E. (1999). Aortic pulse wave velocity as a marker of cardiovascular risk in hypertensive patients. *Hypertension* 33, 1111-1117. doi:10.1161/01.HYP.33.5.1111

Bordeleau, F., Mason, B. N., Lollis, E. M., Mazzola, M., Zanotelli, M. R., Somasegar, S., Califano, J. P., Montague, C., Lavalley, D. J., Huynh, J. et al. (2017). Matrix stiffening promotes a tumor vasculature phenotype. *Proc. Natl Acad. Sci. USA* 114, 492-497. doi:10.1073/pnas.1613855114

Breckenridge, M. T., Desai, R. A., Yang, M. T., Fu, J. and Chen, C. S. (2013). Substrates with engineered step changes in rigidity induce traction force polarity and durotaxis. *Cell. Mol. Bioeng.* 7, 26-34. doi:10.1007/s12195-013-0307-6

Breslin, J. W., Zhang, X. E., Worthylake, R. A. and Souza-Smith, F. M. (2015). Involvement of local lamellipodia in endothelial barrier function. *PLoS ONE* 10, 1-30. doi:10.1371/journal.pone.0117970

Califano, J. P. and Reinhart-King, C. A. (2010). Exogenous and endogenous force regulation of endothelial cell behavior. *J. Biomech.* 43, 79-86. doi:10.1016/j.jbiomech.2009.09.012

Ghibaudo, M., Saez, A., Trichet, L., Xayaphoummine, A., Browaeys, J., Silberzan, P., Buguin, A. and Ladoux, B. (2008). Traction forces and rigidity sensing regulate cell functions. *Soft Mat.* 4, 1836. doi:10.1039/b804103b

Giannotta, M., Trani, M. and Dejana, E. (2013). VE-cadherin and endothelial adherens junctions: active guardians of vascular integrity. *Dev. Cell.* 26, 441-454. doi:10.1016/j.devcel.2013.08.020

Gonzalez, A. M., Cyrus, B. F. and Muller, W. A. (2016) Targeted Recycling of the Lateral Border Recycling Compartment Precedes Adherens Junction Dissociation during Transendothelial Migration. *Am. J. Pathol.* 186, 1387-1402. doi:10.1016/j.ajpath.2016.01.010

Hardin, C. C., Chattoraj, J., Manomohan, G., Colombo, J., Nguyen, T., Tambe, D., Fredberg, J. J., Birukov, K., Butler, J. P., Del Gado, E. et al. (2018). Long-range stress transmission guides endothelial gap formation. *Biochem. Biophys. Res. Commun.* 495, 749-754. doi:10.1016/j.bbrc.2017.11.066

Huveneers, S., Oldenburg, J., Spanjaard, E., Van Der Krogt, G., Grigoriev, I., Akhmanova, A., Rehmann, H. and De Rooij, J. (2012). Vinculin associates with endothelial VE-cadherin junctions to control force-dependent remodeling. *J. Cell Biol.* 196, 641-652. doi:10.1083/jcb.201108120

Huynh, J., Nishimura, N., Rana, K., Peloquin, J. M., Califano, J. P., Montague, C. R., King, M. R., Schaffer, C. B. and Reinhart-King, C. A. (2011). Age-related intimal stiffening enhances endothelial permeability and leukocyte transmigration. *Sci. Transl. Med.* 3, 112ra122. doi:10.1126/scitranslmed.3002761

Janmey, P. A., Fletcher, D. A. and Reinhart-King, C. A. (2019). Stiffness sensing in cells and tissues. *Physiol. Rev.* 100, 695-724. doi:10.1152/physrev.00013.2019

Kohn, J. C., Chen, A., Cheng, S., Kowal, D. R., King, M. R. and Reinhart-King, C. A. (2016). Mechanical heterogeneities in the subendothelial matrix develop with age and decrease with exercise. *J. Biomech.* 49, 1447-1453. doi:10.1016/j.jbiomech.2016.03.016

Krishnan, R., Klumpers, D. D., Park, C. Y., Rajendran, K., Trepat, X., Van Bezu, J., Van Hinsbergh, V. W. M., Carman, C. V., Brain, J. D., Fredberg, J. J. et al. (2011). Substrate stiffening promotes endothelial monolayer disruption through enhanced physical forces. *Am. J. Physiol. Cell Physiol.* 300, C146-C154. doi:10.1152/ajpcell.00195.2010

Lampi, M. C., Faber, C. J., Huynh, J., Bordeleau, F., Zanotelli, M. R. and Reinhart-King, C. A. (2016). Simvastatin ameliorates matrix stiffness-mediated endothelial monolayer disruption. *PLoS ONE* 11, 1-20. doi:10.1371/journal.pone.0147033

Lampi, M. C., Guvendiren, M., Burdick, J. A. and Reinhart-King, C. A. (2017). Photopatterned hydrogels to investigate endothelial cell response to matrix stiffness heterogeneity. *ACS Biomater. Sci. Eng.* 3, 3007-3016. doi:10.1021/acsbiomaterials.6b00633

Lampugnani, M. G., Corada, M., Caveda, L., Breviario, F., Ayalon, O., Geiger, B. and Dejana, E. (1995). The molecular organization of endothelial cell to cell junctions: differential association of plakoglobin, beta-catenin, and alpha-catenin with vascular endothelial cadherin (VE-cadherin). *J. Cell Biol.* 129, 203-217. doi:10.1083/jcb.129.1.203

Le Duc, Q., Shi, Q., Blonk, I., Sonnenberg, A., Wang, N., Leckband, D. and De Rooij, J. (2010). Vinculin potentiates E-cadherin mechanosensing and is recruited to actin-anchored sites within adherens junctions in a myosin II-dependent manner. *J. Cell Biol.* 189, 1107-1115. doi:10.1083/jcb.201001149

Lemmon, C. A., Sniadecki, N. J., Ruiz, S. A., Tan, J. L., Romer, L. H. and Chen, C. S. (2005). Shear force at the cell-matrix interface: enhanced analysis for microfabricated post array detectors. *Mech. Chem. Biosyst.* 2, 1-16.

Liu, Z., Tan, J. L., Cohen, D. M., Yang, M. T., Sniadecki, N. J., Ruiz, S. A., Nelson, C. M. and Chen, C. S. (2010). Mechanical tugging force regulates the size of cell-cell junctions. *Proc. Natl Acad. Sci. USA* 107, 9944-9949. doi:10.1073/pnas.0914547107

Martinelli, R., Zeiger, A. S., Whitfield, M., Sciuto, T. E., Dvorak, A., Van Vliet, K. J., Greenwood, J. and Carman, C. V. (2014). Probing the biomechanical contribution of the endothelium to lymphocyte migration: diapedesis by the path of least resistance. *J. Cell Sci.* 127, 3720-3734. doi:10.1242/jcs.148619

Muhamed, I., Wu, J., Sehgal, P., Kong, X., Tajik, A., Wang, N. and Leckband, D. E. (2016). E-Cadherin-mediated force transduction signals regulate global cell mechanics. *J. Cell Sci.* 129, 1843-1854. doi:10.1242/jcs.185447

Mui, K. L., Chen, C. S. and Assoian, R. K. (2016). The mechanical regulation of integrin-cadherin crosstalk organizes cells, signaling and forces. *J. Cell Sci.* 129, 1093-1100. doi:10.1242/jcs.183699

Paszek, M. J., Zahir, N., Johnson, K. R., Lakins, J. N., Rozenberg, G. I., Gefen, A., Reinhart-King, C. A., Margulies, S. S., Dembo, M., Boettiger, D. et al. (2005). Tensional homeostasis and the malignant phenotype. *Cancer Cell* 8, 241-254. doi:10.1016/j.ccr.2005.08.010

Pelham, R. J. J. and Wang, Y.-L. (1997). Cell locomotion and focal adhesions are regulated by the mechanical properties of the substrate. *Proc. Natl Acad. Sci. USA* 94, 13661-13665. doi:10.1073/pnas.94.25.13661

Peloquin, J., Huynh, J., Williams, R. M. and Reinhart-King, C. A. (2011). Indentation measurements of the subendothelial matrix in bovine carotid arteries. *J. Biomech.* 44, 815-821. doi:10.1016/j.jbiomech.2010.12.018

Pulous, F. E., Grimsley-Myers, C. M., Kansal, S., Kowalczyk, A. P. and Petrich, B. G. (2019). Talin-dependent integrin activation regulates VE-cadherin localization and endothelial cell barrier function. *Circ. Res.* 124, 891-903. doi:10.1161/CIRCRESAHA.118.314560

Rabodzey, A., Alcaide, P., Luscinskas, F. W. and Ladoux, B. (2008). Mechanical forces induced by the transendothelial migration of human neutrophils. *Biophys. J.* 95, 1428-1438. doi:10.1529/biophysj.107.119156

Riveline, D., Zamir, E., Balaban, N. Q., Schwarz, U. S., Ishizaki, T., Narumiya, S., Kam, Z., Geiger, B. and Bershadsky, A. D. (2001). Focal contacts as mechanosensors: Externally applied local mechanical force induces growth of focal contacts by an mDia1-dependent and ROCK-independent mechanism. *J. Cell Biol.* 153, 1175-1185. doi:10.1083/jcb.153.6.1175

Rodríguez-Franco, P., Brugués, A., Marín-Llauradó, A., Conte, V., Solanas, G., Batlle, E., Fredberg, J. J., Roca-Cusachs, P., Sunyer, R. and Trepat, X. (2017). Long-lived force patterns and deformation waves at repulsive epithelial boundaries. *Nat. Mater.* 16, 1029-1036. doi:10.1038/nmat4972

Rosenfeld, D., Landau, S., Shandalov, Y., Raindel, N., Freiman, A., Shor, E., Blinder, Y., Vandenburgh, H. H., Mooney, D. J. and Levenberg, S. (2016). Morphogenesis of 3D vascular networks is regulated by tensile forces. *Proc. Natl Acad. Sci. USA* 113, 3215-3220. doi:10.1073/pnas.1522273113

Stroka, K. M. and Aranda-Espinoza, H. (2011). Endothelial cell substrate stiffness influences neutrophil transmigration via myosin light chain kinase-dependent cell contraction. *Blood* **118**, 1632-1640. doi:10.1182/blood-2010-11-321125

Stutchbury, B., Atherton, P., Tsang, R., Wang, D.-Y. and Ballestrem, C. (2017). Distinct focal adhesion protein modules control different aspects of mechanotransduction. *J. Cell Sci.* **130**, 1612-1624. doi:10.1242/jcs.195362

Sutton-Tyrrell, K., Najjar, S. S., Boudreau, R. M., Venkitachalam, L., Kupelian, V., Simonsick, E. M., Havlik, R., Lakatta, E. G., Spurgeon, H., Kritchevsky, S. et al. (2005). Elevated aortic pulse wave velocity, a marker of arterial stiffness, predicts cardiovascular events in well-functioning older adults. *Circulation* **111**, 3384-3390. doi:10.1161/CIRCULATIONAHA.104.483628

Tan, J. L., Tien, J., Pirone, D. M., Gray, D. S., Bhadriraju, K. and Chen, C. S. (2003). Cells lying on a bed of microneedles: an approach to isolate mechanical force. *Proc. Natl. Acad. Sci. USA* **100**, 1484-1489. doi:10.1073/pnas.0235407100

Urbano, R. L., Furia, C., Basehore, S. and Clyne, A. M. (2017). Stiff substrates increase inflammation-induced endothelial monolayer tension and permeability. *Biophys. J.* **113**, 645-655. doi:10.1016/j.bpj.2017.06.033

Valent, E. T., van Nieuw Amerongen, G. P., van Hinsbergh, V. W. M. and Hordijk, P. L. (2016). Traction force dynamics predict gap formation in activated endothelium. *Exp. Cell Res.* **347**, 161-170. doi:10.1016/j.yexcr.2016.07.029

Vanderburgh, J. A. and Reinhart-King, C. A. (2018). The role of age-related intimal remodeling and stiffening in atherosclerosis. *Adv. Pharmacol.* **81**, 365-391. doi:10.1016/bs.apha.2017.08.008

Vanderburgh, J. A., Hotchkiss, H., Potharazu, A., Taufalele, P. V. and Reinhart-King, C. A. (2018). Substrate stiffness heterogeneities disrupt endothelial barrier integrity in a micropillar model of heterogeneous vascular stiffening. *Integr. Biol.* **10**, 734-746. doi:10.1039/C8IB00124C

Weisbrod, R. M., Shiang, T., Al Sayah, L., Fry, J. L., Bajpai, S., Reinhart-King, C. A., Lob, H. E., Santhanam, L., Mitchell, G., Cohen, R. A. et al. (2013). Arterial stiffening precedes systolic hypertension in diet-induced obesity. *Hypertension* **62**, 1105-1110. doi:10.1161/HYPERTENSIONAHA.113.01744

Yang, M. T., Fu, J., Wang, Y.-K., Desai, R. A. and Chen, C. S. (2011). Assaying stem cell mechanobiology on microfabricated elastomeric substrates with geometrically modulated rigidity. *Nat. Protoc.* **6**, 187-213. doi:10.1038/nprot.2010.189

Yao, L., Caldwell, R. B., Yao, L., Romero, M. J., Toque, H. A. and Caldwell, R. W. (2010). The role of rhoA/rho kinase pathway in endothelial dysfunction. *J. Cardiovasc. Dis. Res.* **1**, 165-170. doi:10.4103/0975-3583.74258

Yeh, Y. T., Serrano, R., François, J., Chiu, J.-J., Li, Y.-S. J., Del Álamo, J. C., Chien, S. and Lasheras, J. C. (2018). Three-dimensional forces exerted by leukocytes and vascular endothelial cells dynamically facilitate diapedesis. *Proc. Natl. Acad. Sci. USA* **115**, 133-138. doi:10.1073/pnas.1717489115

Yeung, T., Georges, P. C., Flanagan, L. A., Marg, B., Ortiz, M., Funaki, M., Zahir, N., Ming, W., Weaver, V. and Janmey, P. A. (2005). Effects of substrate stiffness on cell morphology, cytoskeletal structure, and adhesion. *Cell Motil. Cytoskelet.* **60**, 24-34. doi:10.1002/cm.20041

Zanotelli, M. R. and Reinhart-King, C. A. (2018). Mechanical forces in tumor angiogenesis. In *Biomechanics in Oncology* (ed. C. Dong, N. Zahir and K. Konstantopoulos), pp. 91-112. Cham: Springer International Publishing.